UNIVERSITY OF TWENTE.

Master Thesis in Bioengineering Technologies

Development of magnetic alginate beads for localized mechanical stimulation in tissue engineering

Alba Rivera Pulido

Examination Committee
Supervisor: Dr. ir Jeroen Rouwkema
Daily supervisor: Msc. Mira El Akkawi
2nd daily supervisor: Msc. Vasileios Trikalitis
External member: Dr. ir Constantinos Goulas

Faculty of Engineering Technology
Department of Biomechanical Engineering
The Vascularization Laboratory

Report number: BE-966

November, 2023

Abstract

Cells receive different signals from the cellular environment that influence their behavior and function. Mechanical stimulation promotes cell proliferation and differentiation to form new tissues, like cartilage and bone. Tissue engineering addresses multiple challenges to provide alternatives for damaged tissues. One of them is to locally offer mechanical stimulation to distinct regions of the tissue to allow for differential tissue development within a single construct. In this project, I developed and characterized magnetic alginate beads, synthesized with different concentrations of iron, to provide an alternative method to facilitate tissue regeneration. An assessment of their properties was performed, from their size and sphericity to their magnetic properties and biocompatibility.

Beads were produced using a syringe pump with different flow rates, nozzles, distances between the nozzle and the supporting bath needed for the crosslinking of the alginate, and stirring speeds. A statistical test based on their size and sphericity was carried out to determine whether the parameters influenced the outcome, suggesting a strong correlation between the distance and the stirring with both the size and sphericity and the nozzle with the diameter. Then, beads were synthesized with 0.2, 1, and 10 % (w/v) of iron, and their magnetic properties were examined in different solution viscosities (1, 10, and 100 cST). For this, the distance speed from the bead toward a magnet was measured, along with a vibrating sample magnetometer (VSM) analysis to determine the actual content of iron present inside the beads. Finally, the biocompatibility of the beads was assessed by culturing C2C12 myoblast cells on cytodex microcarriers and conducting a live dead assay at multiple time points (1, 3, and 7 days) to evaluate the cell viability and interaction with the magnetic beads. Overall, the characterization of magnetic alginate beads provides insights into their properties and possible applications in tissue engineering, specifically in inducing mechanical stimulation and therefore, guiding cell differentiation for tissue regeneration.

Acknowledgements

I want to thank the committee: Jeroen, Mira, Vasileios and Constantinos. I am so grateful for having been part of this close group where I felt comfortable to reach them when I needed guidance with my project. Especially to Mira, who has always been present and patient, and whose enthusiastic energy infected me and made my learning process much more enjoyable.

Also, I want to thank my friends, who have been my supporting network throughout the process. To Sandra, Salma and Cristina, who have been listening to my ideas when I was stuck and offered me their help. To Eli, Maisa and Jaimie, with whom it would not have been possible to work better during the master. To Carlotta and Swathi, who helped me in the lab when needed. Thank you for being my family by choice being far from home.

Lastly, I want to thank my parents, for always having trusted me even more than I did myself. To my mom, for her infinite support with everything. And especially to my father, who sadly is no longer with us, but without whom I would not have come to study this master's in The Netherlands.

Contents

List of Figures

List of Tables

List of abbreviations

ECM Extracellular matrix
GF Growth factors
MSCs Mesenchymal stem cells
iPSCs Induced pluripotent stem cells
Ex vivo outside an organism
MNPs Magnetic nanoparticles
ANOVA Analysis of variance
SPSS Statistical Package for the Social Sciences
XRD X-ray diffraction
PMMA Polymethyl methacrylate
cSt Centistokes
VSM Vibrating Sample Magnetometer
PPMS Physical Property Measurement System
DMEM Dulbecco's Modified Eagle Medium
FBS Fetal bovine serum
Pen/strep Penicillin/streptomycin
DPBS Dulbecco's Phosphate Buffered Saline
Calcein-AM Calcein-acetoxymethyl ester
PI Propidium iodide
SD Standard deviation

1

Introduction

1.1 Tissue engineering: the future of regenerative medicine

Tissues within the body are constantly renewing. These tissues can be damaged in a way that the body is not capable of repairing them, and here is where tissue engineering comes into play. Tissue engineering is a field within regenerative medicine that focuses on the regeneration of damaged tissues or providing alternative solutions to replace them from outside the body [1]. It can provide artificial tissues for a wide range of clinical applications, such as those related to conditions like osteoarthritis [2], bone fractures [3], burns [4], and organ transplants [5], as well as for drug testing and disease models [6].

In the context of organ transplantation, for instance, tissue engineering emerges as a transformative solution. Organ transplantation has become a treatment to address end-stage organ failures [7]. However, there are two main challenges in this field: donor shortage and immunosuppression. There are not enough organs available for transplantation, which implies a high mortality rate for those patients on the waiting list. Also, there is the risk of rejection and the necessity for lifelong immunosuppressive drugs, which come with their associated hazards such as infections, toxicity, and side effects, leading to a decrease in life expectancy of approximately 10 years [8]. Tissue engineering can solve these problems by providing organs engineered ex vivo [9].

On the one hand, bioartificial organs can be built by decellularizing a donor organ to obtain a scaffold, which can be recellularized with autologous differentiated cells, taking advantage of the vascular network already present in the scaffold and eliminating the problem of rejection and immunosuppression [7, 10]. On the other hand, it is also possible to produce synthetic biodegradable scaffolds, avoiding the main problems of conventional organ transplantations [11]. Nevertheless, artificial tissues present numerous hurdles, such as vascularization or controlling cell behavior.

Blood vessels are the highways to transport nutrients and oxygen, as well as removing waste products, which is essential to keep the tissue alive. These vessels are divided into capillaries, with a distance between them below 200 µm to allow proper oxygen and nutrient diffusion [12]. In engineered constructs, the distance between capillaries exceeds the optimal limit, restricting the diffusion processes needed to maintain the viability of the tissue. This results in longer distances for molecules to travel, slowing down the diffusion process and leading to insufficient consumption of nutrients and oxygen by

the tissue to maintain efficiency [13].

Bioreactors, devices that simulates the biological environment in a controlled manner, can improve the nutrient and oxygen delivery through perfusion systems. This type of bioreactors pump the culture medium through the construct rather than around it, enabling the delivery of nutrients and oxygen by both diffusion and convection [13]. While the use of bioreactors to produce a dynamic in vitro microenvironment has been a significant breakthrough, allowing to maintain tissues alive, once these tissues are implanted, their viability is compromised [8, 12].

Furthermore, controlling cell behaviour is another challenge within the tissue engineering field. The surroundings of cells have a significant impact on their behaviour, influencing how cells respond and function. The cell behaviour relies significantly on the physical, chemical, and biological cues present in the cellular environment. This environment includes the extracellular matrix (ECM), surronding cells and molecules like cytokines and hormones [14]. Cell-ECM and cell-cell interactions regulate cellular behavior. The ECM provides anchorage for cells through surface proteins (integrins) and helps with cell migration. Besides, environmental signals are transmitted through the ECM, influencing cell proliferation, differentiation, and apoptosis [15].

The main components needed in tissue engineering are cells, which can come directly from the patient or from stem cells; scaffolds, biodegradable templates designed to mimic the ECM for cell expansion and organization into tissue structures; and growth factors (GF), used to stimulate cell proliferation and differentiation, among other functions, by transmitting environmental signals. Cells are cultured on these scaffolds under the proper conditions. This encourages the formation of a tissue construct that can be implanted in vivo to replace the damaged one [1, 16].

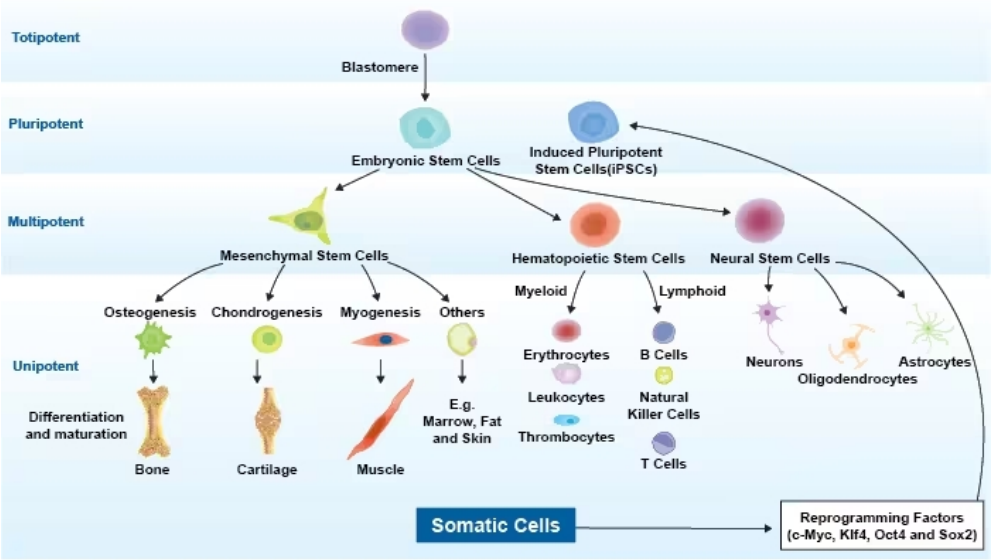

Figure 1.1: Stem cell diversity[1]and their differentiation potential

[1]Note: There are more multipotent stem cell types that are not included in the image.

When it comes to forming the new engineered tissue, differentiated cells are required to proliferate in these scaffolds. These differentiated cells can be obtained through stem cells, such as mesenchymal stem cells (MSCs) or induced pluripotent stem cells (iPSCs). Stem cells have the ability of self-renewal and to differentiate into different cell types depending on their potency (Figure 1.1 [17]). These properties define the stemness of stem cells. The differentiation process is possible thanks to their inherent plasticity, a key factor for stem cell therapies, along with the extracellular regulatory signals that control their proliferation and differentiation [14, 18].

Different intricated stimuli participate in cell differentiation, such as transcription factors, GF, physical factors, etc., guiding cells towards specific lineages. All these factors regulate the intertwined signaling pathways, where the extracellular signals are integrated within the cell to activate or inhibit specific molecular processes that will lead to the cellular specialization [19]. The integration of mechanical signals, known as mechanotransduction, has an important role in cell differentiation.

1.2 Mechanotransduction in cell differentiation

Mechanotransduction is the process by which external mechanical forces are transformed into intracellular biochemical signals (Figure 1.2[20]). These signals activate different signaling pathways, altering the gene expression and cellular structure, thereby regulating cell behavior and fate [21, 22]. Mechanical stress influences cellular differentiation, increasing osteogenic, chondrogenic, and neuronal tissue development [23, 24], for instance.

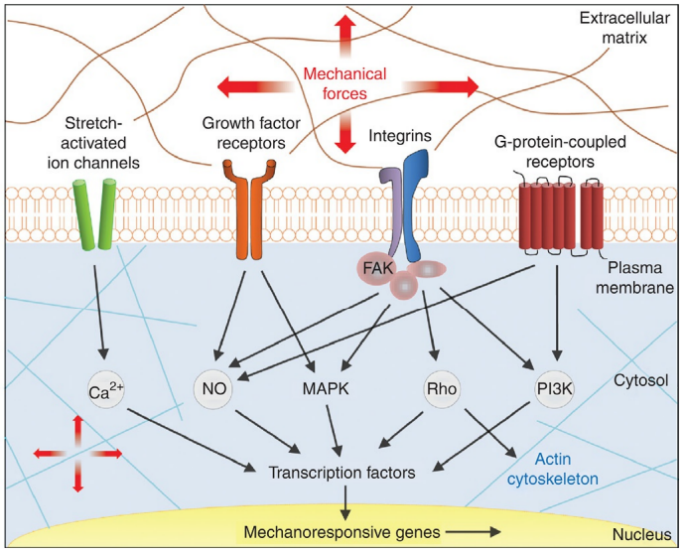

Figure 1.2: Mechanotransduction: mediators involved in translating extracellular mechanical signals into intracellular biochemical signals.

The signal integration process is crucial in guiding cells toward specific lineages during differentiation. MSCs have the ability to transform into different cell types, such as myoblasts (muscle), chondrocytes (cartilage) or osteoblasts (bone). The differentiation process to these specialized cell types is controlled by specific transcription factors, like MyoD for muscle, Runx2 for bone, or Sox9 for cartilage [21]. By regulating the stimuli the cells receive, it is possible to control the differentiation process.

Cells adhere to the ECM through focal adhesions, formed by transmembrane proteins called integrins that link the ECM to the cytoskeleton. These integrins, along with ion channels and protein receptors, are responsible for translating the external signals to activate or inhibit the signaling pathways that will lead to specific transcription factors [25]. Thus, depending on the stimuli

the cell senses and the factors that are reached, cells will transform into one type or another.

There are different strategies to apply external mechanical stimuli. One of the most common ones is through mechanical bioreactors, providing controlled compression, cyclic tension, or shearing to artificial tissues. Fluid dynamic stress (shear stress) is produced by the fluid around the construct, and it is considered the primary mechanical stimulus to activate the mechanotransduction process. However, the mechanical forces involved in the bioreactor actuate on the whole scaffold, making it impossible to stimulate specific regions of the tissue [23, 26].

Other approaches to providing mechanical localized stimulation include magnetic hydrogels. Among its applications in tissue engineering, hydrogels with magnetic nanoparticles (MNPs) offer an alternative way to manipulate mechanotransduction pathways to regulate stem cell differentiation. Polymeric biomaterial particles can facilitate the stimulation of cells and subsequently their differentiation into a specific tissue type. The use of an external magnetic stimulus allows, by using the particle as the probe, the remote, local, mechanical stimulation of cells and tissues [27, 28].

1.3 Magnetic hydrogels

Hydrogels are 3D networks of polymer chains that have the ability to absorb water. Their properties allow them to swell and hold water while maintaining their structural integrity and mechanical properties. Their versatile features make them suitable for a broad variety of applications within the biomedical field and pharmaceutical industry. From contact lenses, artificial skin, and scaffolds, to drug delivery, to mention a few [29].

Alginate is a natural anionic polysaccharide obtained from brown algae, and it is widely used as a biomaterial in tissue engineering due to its biocompatibility, biodegradability, non-toxicity, and flexibility properties. There are different approaches to producing alginate hydrogels (See figure 1.3[30]), involving a crosslinking process where chemical reactions form bonds between polymer chains. These chemical interactions can be reversible (non-covalent bonds) or irreversible (covalent bonds), controlling the degradability of the hydrogel [30].

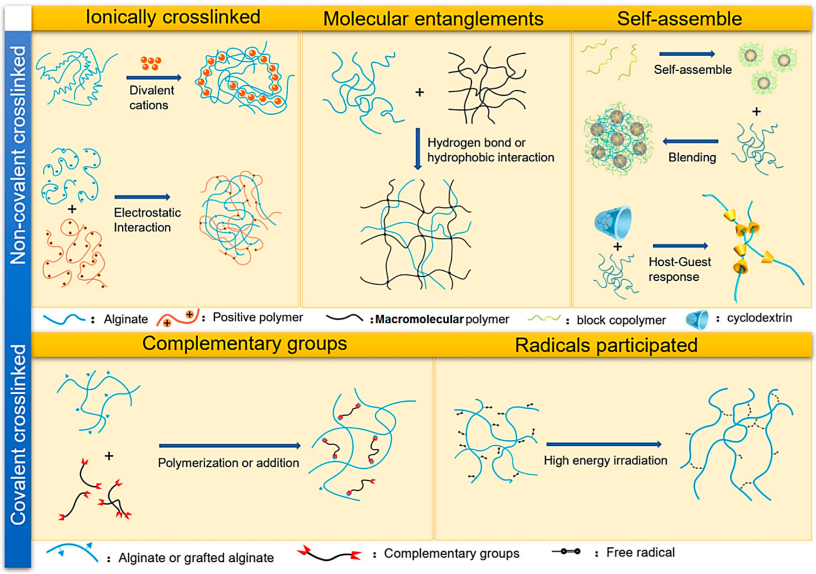

Figure 1.3: Crosslinking approaches to form alginate hydrogels.

Ionic crosslinking with positively charged ions, such as Ca^{2+} or Mg^{2+}, is the easiest and most cost-effective method to form this hydrogel [30]. Furthermore, it has been reported that alginate being crosslinked by 2% (w/v) calcium chloride had the best performance regarding its properties [31]. Also, the presence of ethanol in the calcium chloride solution (below 30% v/v) presents several benefits, like enhanced surface homogeneity or mechanical properties [32].

Several studies have demonstrated the potential of applying magnetic nanoparticles in tissue engineering, particularly for bone and cartilage regeneration through magnetic stimulation [23, 33]. The production of spherical microgels has also been examined, whether coated with MNPs and designed to controllably release encapsulated substances [34] or MNPs embedded inside alginate beads for local micro-actuation of tissue constructs [35]. However, the use of iron oxide nanoparticles encapsulated in beads provides limited mechanical force to stimulate the cells and presents a contamination risk of the surrounding cells due to leakage of iron oxide nanoparticles in the medium.

Extrusion dripping is a common and easy technique to produce alginate beads. By this method, extruded droplets of alginate are crosslinked in a supporting bath containing cations. Their sizes are usually greater than 1 mm and their sphericity has an impact on the mechanical and chemical stability [36]. To prevent shape deformation during the process, the viscosity and surface tension of the calcium chloride solution should be reduced. Introducing a surfactant into the solution can enhance the bead penetration, contributing to its spherical formation. [37].

The development of responsive magnetic hydrogels makes it possible to aid with differentiation and tissue regeneration. The investigation of magnetic alginate beads to provide localized mechanical stimulation entails a new approach for more effective strategies in tissue engineering.

1.4 Research goal and Objectives

Considering the challenges within tissue engineering, particularly in understanding and controlling cell behavior, it is essential to influence cell fate and differentiation for regenerative medicine. This project aims to produce magnetic alginate beads as an option to indirectly stimulate cells mechanically to facilitate artificial tissue development. To guide the investigation, the research goal is addressed by defining specific objectives.

Research goal:

To develop and activate magnetic alginate beads to provide localized mechanical stimulation to cells with the purpose of inducing differential tissue development.

Objectives:

1. Production and process optimization of magnetic alginate beads with different weight fractions of iron particles.

2. Determine the magnetic response of magnetic alginate beads depending on their iron weight fractions.

3. Evaluate the biocompatibility of magnetic alginate beads.

4. Assess the effects of magnetic stimulation on cell behavior.

2

Experimental Methods

2.1 Materials

Reagents: Sodium alginate (Alginic acid sodium salt from brown algae), Calcium chloride dihydrate powder ($CaCl_2.2H_2O$), silicon oils with different viscosities, Cytodex 3 microcarrier beads and Live/Dead Cell Double Staining Kit were purchased from Sigma-Aldrich. Iron powder, Dulbecco's Phosphate Buffered Saline (DPBS) and Dulbecco's Modified Eagle Medium (DMEM) were obtained from Thermo Scientific. Optiprep for the iron suspension was purchased from Stem Cell Technologies.

Disposables: The nozzles used to extrude the alginate solutions were purchased from Needlez. To filter alginate solutions acrodisc 32 mm syringe filters with 0.45 μm supor membrane (PALL Life Science) were used. 60 mL syringes were obtained from Mediware. Sarstedt Inc Transfer Pipette (3.5ml, Graduated) was used for mixing the iron within the alginate solution.

Equipment: The syringe pump (PHD Ultra, Harvard Apparatus) was used to produce the beads. The EVOS microscope (Invitrogen EVOS FL Imaging System - Thermo fisher Scientific) was used for all the imaging. The Sartorius scale was used to weigh alginate and iron powders. The magnetic stirrer IKA C-MAG HS 7 (Sigma-Aldrich) was used to mix alginate solutions, whereas IKA color squid bubbles magnetic stirrer (Boom B.V. Meppel) was used for the synthesis of the alginate beads. MilliQ-water was obtained from Purelab flex (Salme en kipp). For the oxidation state, the X-ray diffraction (XRD) analysis was performed using the D8 Discover apparatus with LYNXEYE XE-T detectors (Bruker). For the bead's magnetic properties, the digital microscope Dino-Lite Edge was used to record the bead's movement toward a magnet. Physical Property Measurement System (PPMS) DynaCool from Quantum Design was used for the VSM analysis. For the cell attachment to microcarriers, the roller mixer RS-TR 5 (Phoenix Instrument) and vortex mixer L46 (Labinco) were used. A bürker-türk counting chamber (Marienfeld Superior) was used for manual cell counting.

2.2 Production of non-magnetic and magnetic Alginate beads

2.2.1 Synthesis of Alginate beads

Alginate beads were produced with different process parameters to optimize the production. Figure 2.1 shows the setup used to produce them. With the syringe pump, the flow rate can be controlled, along

with the target volume. 2% (w/v) of sodium alginate powder was weighed and dissolved in Milli-Q using a magnetic stirrer. The solution was filtered and introduced into a 60 mL syringe, which was fixed on top of the the syringe pump. Extrusion nozzle inner diameter and the distance between the nozzle tip and the crosslinking solution surface influence respectively the diameter and sphericity of the beads, with particular emphasis on the importance of the sphericity as it is directly correlated with bead homogeneity [36, 37]. The supporting bath (0.18 M) consists of 2% (w/v) of calcium chloride [31] and 10% (v/v) of ethanol with 70% purity. The website handymath [38] was used for the ethanol calculations. Underneath this solution, a magnetic stirrer was placed for proper crosslinking of the alginate, and the stirring speed is another parameter that can be controlled.

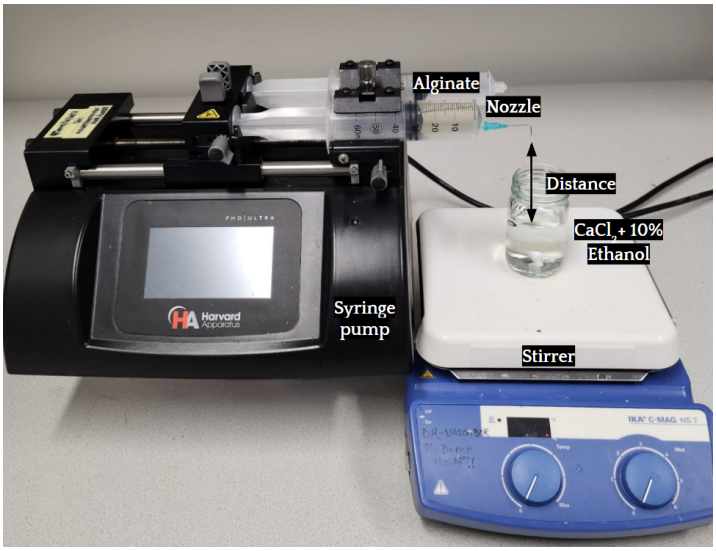

Figure 2.1: Syringe pump setup to produce Alginate beads

To study the impact of these parameters, we selected minimum and maximum values for each, guided by relevant literature [37]. Davarcı et al. (2017) identified specific parameter ranges in their study, such as a minimum distance of 2.5 cm to obtain a spherical shape. The chosen minimum and maximum values, presented in table 2.1, were determined based on their findings. From these parameters, 12 combinations were chosen for the production of the beads. Finally, the beads were stirred for at least 30 minutes in calcium chloride before rinsing them with Milli-Q and stored at 4ºC.

Parameters	**Min value**	**Max value**
Flow rate (ml/h)	25	150
Nozzle (G) (Inner diameter)	27 (0.21 mm)	23 (0.33 mm)
Distance (cm)	3	30
Stirring speed (rpm)	100	500

Table 2.1: Minimum and maximum selected parameter values to study their influence.

2.2.2 Synthesis of magnetic Alginate beads

To produce magnetic Alginate beads, the setup was the same as in figure 2.1, with the difference that now the solution within the syringe contains iron. The higher density of iron compared to alginate results in its sedimentation over time. This would lead to a gradual depletion of iron in the bead production, meaning that the first beads produced would have more iron content than the last ones.

To improve the homogeneity of the iron distribution, the viscosity of the solution was increased by raising the alginate content and dissolving it in 45% Optiprep.

To study whether the viscosity of the solution and the iron content influence in the formation of the beads, different combinations of alginate with Fe were produced. 2% (w/v) of alginate was mixed with 0.2 and 1% (w/v) of iron and 3% (w/v) of alginate was mixed with 0.2, 1 and 10% (w/v) of iron. These solutions were blended using a shaker and a plastic pipette. Although this method does not allow a completely homogeneous distribution of the iron particles through the alginate due to the difference in densities, it was enough to produce magnetic beads. A flow rate of 150 ml/h was used, along with both 23G and 27G nozzles. The distance was set to 3 cm and the supporting bath did not undergo stirring, as this ended up in the deformation of the beads or their attachment to the magnet.

2.3 Characterization of non-magnetic and magnetic Alginate beads

2.3.1 Size and sphericity

From each experimental condition, a total of 10 samples were collected to analyze and evaluate the size and sphericity. The EVOS microscope was used to take the pictures of these 10 beads and the software ImageJ was used to measure their diameters. Per each sample of each condition, different positions from the bead were set manually to obtain a few different diameters (at least 6 as shown in figure 2.2), from which the least and greatest were selected to obtain the size, by getting the average diameters. With this diameter, the volume of the beads could be determined from the equation 2.1, where V_{bead} is the volume and d the average diameter. To obtain the bead's shape, the sphericity (Φ) was calculated based on the equation 2.2, where d_{min} and d_{max} are the minimum and maximum diameters measured respectively. Bead shapes are considered spherical for values above 0.95, while between 0.9 and 0.95 they are considered oval or with a pear shape, and under 0.9 they are not spherical [37].

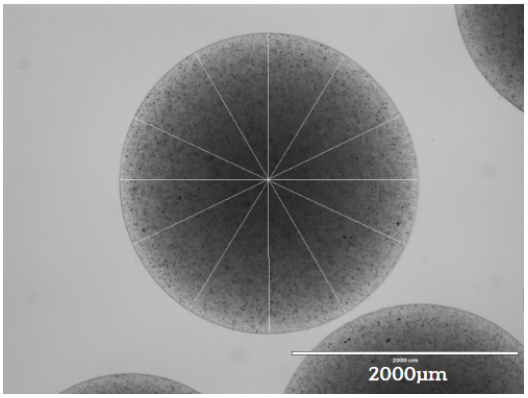

Figure 2.2: Diameter measurements in ImageJ from multiple positions for accuracy

$$V_{\text{bead}}(\text{mL}) = \frac{4}{3}\pi\left(\frac{d}{2}\right)^3 \frac{1}{1000} \tag{2.1}$$

$$\Phi = \frac{2d_{\text{min}}}{d_{\text{min}} + d_{\text{max}}} \tag{2.2}$$

Additionally, after collecting these data, a statistical analysis was performed using the SPSS software to determine which factors influence the sphericity and diameter. The statistical significance of these

parameters was evaluated through an analysis of variance (ANOVA) using the F-test, where a significance level of $p < 0.05$ was considered. A detailed step by step procedure using the SPSS software is outlined in Appendix A. When the p-value associated with the explanatory variable is less than 0.05, it means that the parameter explains the variance of the outcome, suggesting a statistically significant relationship between the dependent and explanatory variables.

2.3.2 Oxidation state

To investigate the iron oxidation state inside the alginate beads, the XRD analysis was performed. This technique provides information about the internal structure of a material by throwing X-rays toward a sample and analyzing the scattering of the radiation produced by the atoms of the sample [39]. This method has been widely used for oxidation characterization [40, 41], allowing us to determine whether the iron of the magnetic beads is oxidized or not.

Figure 2.3: X-ray diffractometer used to analyze the oxidation state of magnetic alginate beads.

The magnetic alginate beads (10 % w/v) were dried for 2 days at room temperature, after which they were placed inside a polymethyl methacrylate (PMMA) mold to go inside the XRD apparatus (See figure 2.3 [42]). Iron powder in its original powder state and encapsulated state inside alginate beads were analyzed and compared to the reference Alpha Iron found in the literature. The 2Theta scans were recorded at room temperature (300K) in angles ranging from 20 to 120 2Theta with a step size of 0.01 2Theta and continuous scan mode.

2.3.3 Magnetic properties

To investigate the magnetic properties of the beads and their possible impact on stimulating cells mechanically, variations in iron content and solution viscosities were introduced. Body fluids have different viscosities. This, along with tissue stiffness and elasticity, determines how cells respond to mechanical stimulations [43]. Therefore, to accurately reflect the potential interactions of the magnetic beads, it was explored how different viscosities affect the magnetic properties.

2.3.3.1 Moving speeds

The moving speed of the magnetic beads towards a magnet was analyzed. Magnetic beads were introduced in recipients containing solutions with different viscosities: 1 cST (milli-Q water), 10 cST (silicon oil), and 100 cST (silicon oil). Beads were produced with 3% (w/v) alginate, 0.2, 1, and 10 % (w/v) of Fe, a flow rate of 150 ml/h, a 23G nozzle, and a distance of 3 cm. Once the bead reached the bottom of the container, due to its high density, a magnet was introduced inside the solution, moving it closer toward the bead until it started moving.

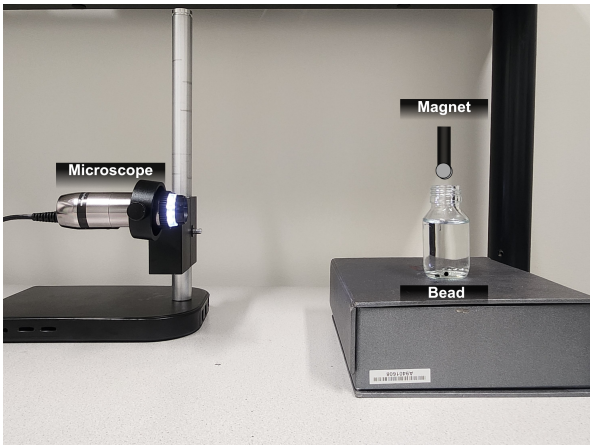

Figure 2.4: Setup to measure the moving speed of magnetic beads towards a magnet in different solution viscosities.

A digital microscope was placed horizontally to record the movement of the bead going upward, until reaching the magnet, as shown in figure 2.4. This method can provide an idea of how the iron content and the viscosity of the medium will impact the moving speed, assessing which factor has more impact on the speed.

To obtain the speed, the distance between the bead and the magnet was measured with the DinoCapture 2.0 software. First, when the bead started being attracted to the magnet, it repositioned itself to align the maximum amount of iron within it to face upward against the magnet. At the point when the bead began to move upward, the bead-magnet distance was measured every 0.1 seconds until the bead reached the magnet. However, in some conditions, it was not possible to measure the distance in each 0.1-second frame as the bead was moving and appeared blurred or the frame remained the same as the previous one, making it impossible to calculate each time-frame speed to get the acceleration. Hence, the speed was calculated as the total distance divided by the total time.

A visual representation of the process is depicted in the figure 2.5. Combining 0.2, 1, and 10 % (w/v) of Fe with 1 cST, 10 cST and 100 cST of viscosity, 9 conditions were evaluated. 5 different beads per condition were used, obtaining the average speed in the end. Due to technical problems, the conditions 0.2% (w/v) 10cST, 0.2 % (w/v) 100cST, and 1 % (w/v) 100cST only counted with the data of 4 beads.

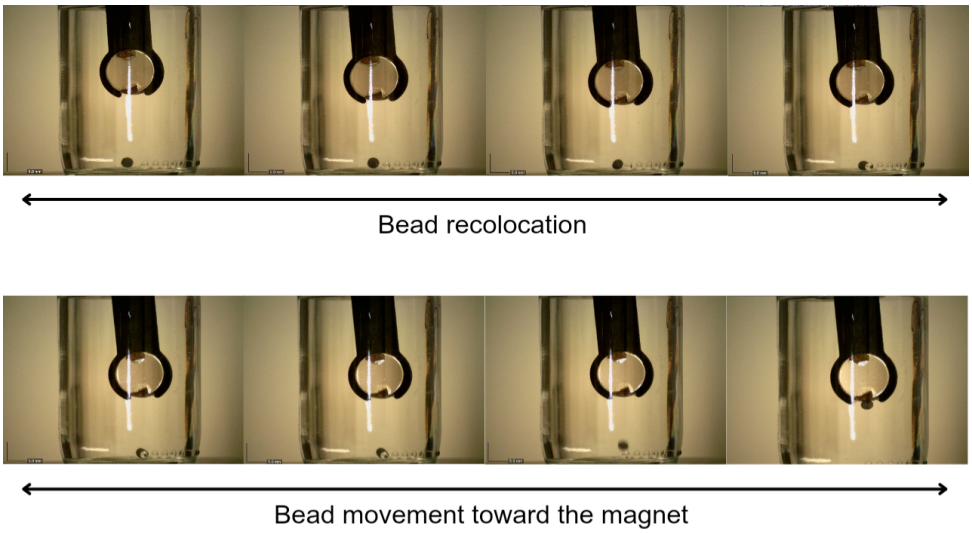

Figure 2.5: Bead movement upon magnet attraction. First, bead recolocation to align the iron to face the magnet. Then, bead movement toward the magnet.

2.3.3.2 VSM analysis

Vibrating-sample magnetometry (VSM) is a technique used to measure the magnetization of a sample when magnetic fields are applied. It is based on Faraday's Law of induction. In a constant magnetic field, the sample is magnetized, and its magnetic dipole moment creates a changing magnetic field that generates an electric current, which is proportional to the sample's magnetization. As a result, a hysteresis curve is obtained, which provides information about the magnetic saturation [44].

The magnetic beads used for the moving speed were analyzed through this method by applying a magnetic field in the 0-2 T range to obtain their magnetic moment saturation. After being dried at room temperature, all 5 beads used per condition, with the exception of 0.2% (w/v) 10cST and 0.2 % (w/v) 100cST where only 4 beads could be analyzed, were incorporated into a plastic capsule. Then, a drop of super glue was applied to prevent them from moving and the capsule was closed. Afterward, a thread was used to wrap the capsule for retrieval from a straw, where it was initially inserted before being placed into the VSM machine, as shown in figure 2.6.

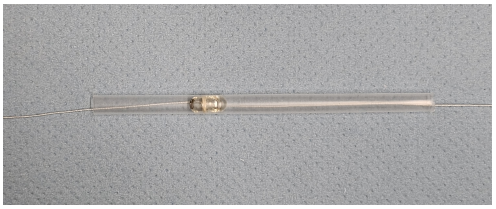

Figure 2.6: Sample preparation for VSM analysis.

As a reference point, in another experiment, we measured the magnetic moment saturation of iron powder in the magnetic field range [-3 T; +3 T]. 4 measurements were done on 4 different iron quantities inside the gelatin capsule. When tracing the maximum magnetic moment obtained for each iron quantity, a linear correlation is obtained with R^2 of 0.9995.

This correlation of the magnetic saturation with the iron content can be used as a regression model, predicting the iron content based on the magnetic saturation of the magnetic beads. As there are multiple beads measured in each condition, the amount of iron obtained from the regression model was divided by the number of beads, getting the grams of iron per bead (M_{Fe}). Aside from this, the volume of the beads was obtained from the equation 2.1. Knowing the grams of iron per bead, the average volume of the bead, and that w/v % corresponds with the grams per 100 mL, the measured weight fraction was calculated using the equation 2.3, after which it was compared with the initial one.

$$\%\ (\mathrm{w/v}) = \frac{M_{\mathrm{Fe}} \times 100}{V_{\mathrm{bead}}} \tag{2.3}$$

2.4 Biocompatibility of magnetic Alginate beads

Magnetic Alginate beads (1% w/v Fe) were integrated to a cell culture to investigate their biocompatibility. C2C12 myoblast cells were thawed from liquid nitrogen and cultured in a T75 flask at a density of 5000 cells/cm^2. Cells were grown and maintained in DMEM culture medium supplemented with 10% (v/v) fetal bovine serum (FBS) and 1% (v/v) penicillin/streptomycin (pen/strep) and placed in

a 37ºC incubator. As the cells will need to be suspended in the medium for the magnetic beads to provide mechanical stimuli, cells were attached to microcarriers.

2.4.1 Cytodex microcarriers and cell attachment

Microcarriers are small spheres with diameters in the range of 100–500 μm that provide a 3D microenvironment for cells, allowing more accurate data compared to 2D culture systems [45]. Following the manufacturer guidelines and recommendations, microcarriers were hydrated in Ca^{2+} and Mg^{2+} free PBS (50 to 100 mL/g of Cytodex) and sterilized overnight in 70% (v/v) ethanol.

This hydration process was carried out for at least 3 hours at room temperature. Subsequently, the microcarriers were washed in fresh PBS (30 to 50 mL/g of Cytodex) for 2-3 minutes and then transferred to new PBS. For the sterilization, microcarriers were washed twice in ethanol (50-100 ml/g Cytodex) and then incubated overnight. The ethanol was removed and the microcarriers were rinsed three times in sterile free PBS (50 ml/g Cytodex) and once in culture medium (20-50 ml/g Cytodex) before use. A stock solution was stored in sterile PBS at 4℃.

For the cell attachment to microcarriers, 2 g/L of cytodex were mixed with 1.10^5 cells/mL in 1/3 of the final culture medium solution to improve the attachment. After 2 hours of incubation at 37ºC, cell attachment was observed under the microscope, and the remaining culture medium was added to reach the proper concentrations.

The ideal technique for the attachment is to use a spinner flask during the incubation process, as explained by the manufacturer. However, no spinner flasks were available, so in order to find out the most effective way for cells to attach to microcarriers, different approaches were assessed: cells with microcarriers were left in the incubator for 2 hours; they were left in the incubator and every 30 minutes they were taken out and vortex for 10 seconds at a low speed; and they were left in the incubator and every 30 minutes they were taken out and placed in the roller mixer for 2 minutes at a low speed. The different condition solutions were visually analyzed under the microscope by adding 10 μL.

2.4.2 Sterilization of magnetic Alginate beads

As the crosslinking process is reversible, sterilization should be carried out carefully to avoid any chemical component that competes with the calcium ions of the bonds between alginate chains. PBS interferes in this process due to the presence of phosphate ions, which exchange with the calcium ones [46], leading to the breakage of alginate-calcium bonds, the swelling of the beads and, thus, their partial degradation.

To sterilize the beads, they were rinsed in 70% (v/v) ethanol for 60 minutes, 30 needed for the ethanol to reach the center of the bead and the rest to eliminate any microorganisms. The 0.18 M calcium chloride solution used for the alginate crosslinking was used to rinse the beads after being filtered with a 0.45 μm syringe filter. Then, beads were rinsed in a new filtered 0.02 M calcium chloride solution and once in DMEM culture medium.

2.4.3 Live Dead Assay and Cell viability

A live-dead assay was performed to investigate the impact of the magnetic beads on cells. Different time points were analyzed: after 1 day, after 3 days, and after 7 days. Per each time point, a 24-well plate was prepared as depicted in figure 2.7, where each well contained 0.5 mL of DMEM culture medium and its respective condition.

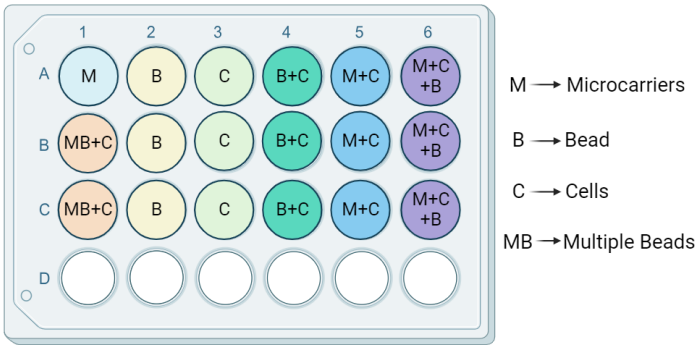

Figure 2.7: Live/Dead Assay scheme with the conditions: 1) M: Just microcarriers; 2) B: Just one bead; 3) C: Just cells; 4) B+C: Cells with one bead; 5) M+C: Cells attached to microcarriers; 6) M+C+B: Cells attached to microcarriers and one bead; 7) MB+C: Cells and 8 beads.

100 μL of a staining solution were added to each well containing cells. This solution combines 10 μL of calcein AM and 5 μL of propidium iodide (PI) per each 5 mL of PBS. Calcein and PI are dyes used to label live and dead cells respectively. Calcein is permeable to the membrane of viable cells and can be transformed by intracellular esterases to produce a green fluorescent signal, whereas PI can only pass through damaged cells and produces a red fluorescence upon binding to DNA [47, 48].

Additionally, a quantitative assessment was performed by staining the cells with trypan blue dye, which is only absorbed by non-viable cells when their membrane is broken down. Cells were cultured at a density of 5000 cells/cm^2 and 3 conditions were evaluated: control with just cells, 1 bead incorporated, and 3 beads incorporated. Live cells were manually counted with a bürker-türk counting chamber after 1, 3, and 7 days, along with a dead cell counting on day 7 to obtain the cell viability.

3

Results & Discussion

3.1 Characterization of non-magnetic and magnetic Alginate beads

3.1.1 Size and sphericity of Alginate beads

Beads were produced under 12 different conditions combining the different parameters that influence the size and shape of the beads. After 10 samples of each one were analyzed and the average diameter and sphericity were calculated, along with the standard deviation, as shown in Table 3.1, the data was plotted (Figure 3.1) based on the different parameters for a proper comparison.

Nozzle (G)	**Distance** (cm)	**Flow-rate** (mL/h)	**Stirring speed** (rpm)	**Diameter** (mm)	**Sphericity** (Φ)
23	3	25	100	2.606 ± 0.02	**0.949 ± 0.02**
23	3	150	500	2.835 ± 0.17	0.820 ± 0.10
23	30	25	100	2.824 ± 0.26	0.812 ± 0.09
23	30	150	500	2.945 ± 0.34	0.646 ± 0.17
27	3	25	100	**2.280 ± 0.06**	**0.951 ± 0.02**
27	3	150	500	**2.305 ± 0.07**	0.911 ± 0.03
27	30	25	100	2.526 ± 0.20	0.830 ± 0.09
27	30	150	500	2.734 ± 0.22	0.647 ± 0.11
23	3	25	500	2.872 ± 0.17	0.709 ± 0.06
23	3	150	100	2.651 ± 0.05	**0.952 ± 0.02**
27	3	25	500	**2.427 ± 0.09**	0.723 ± 0.05
27	3	150	100	**2.322± 0.02**	**0.954 ± 0.01**

Table 3.1: Size and sphericity (data are presented as mean ± SD) of Alginate beads based on different parameter values. Outcomes represented in blue: smallest diameters and highest sphericities.

Regarding the outcome based on the nozzle (Figure 3.1 A), the sphericity appears to exhibit minimal variation, from 0.81 for 23 G to 0.84 for 27 G. However, in terms of the diameter, it was observed that when the smallest nozzle was used, there was a reduction in diameter, from 2.79 mm to 2.43 mm. This finding is reasonable as the inner diameter of the nozzle plays a crucial role in determining the size.

Looking into the distance parameter (Figure 3.1 B), it is evident that employing the minimum distance yields better results in terms of both sphericity and diameter. We observe higher spherical values, 0.87 for a 3 cm distance compared to 0.73 for a distance of 30 cm, and smaller diameters, 2.54 mm for the minimum distance compared to 2.76 mm.

Focusing now on the flow rate (Figure 3.1 C), upon initial observation, there appears to be minimal variation, with a slight improvement when using the minimum flow rate. When beads were produced at 25 ml/h, sphericity was 0.83 and the diameter 2.59 mm, while when using a flow rate of 150 ml/h, a sphericity value of 0.82 and a diameter of 2.63 mm were obtained. However, the overall impact on the results is not clear enough to affirm that one flow rate is better than the other.

Lastly, for the stirring speed (Figure 3.1 D), when using the lowest speed, the sphericity increases, and the diameter is reduced. It is clearly better when 100 rpm was used, obtaining a sphericity value of 0.91 and a diameter of 2.53 mm, compared to values of 0.74 and 2.69 mm when stirred at 500 rpm.

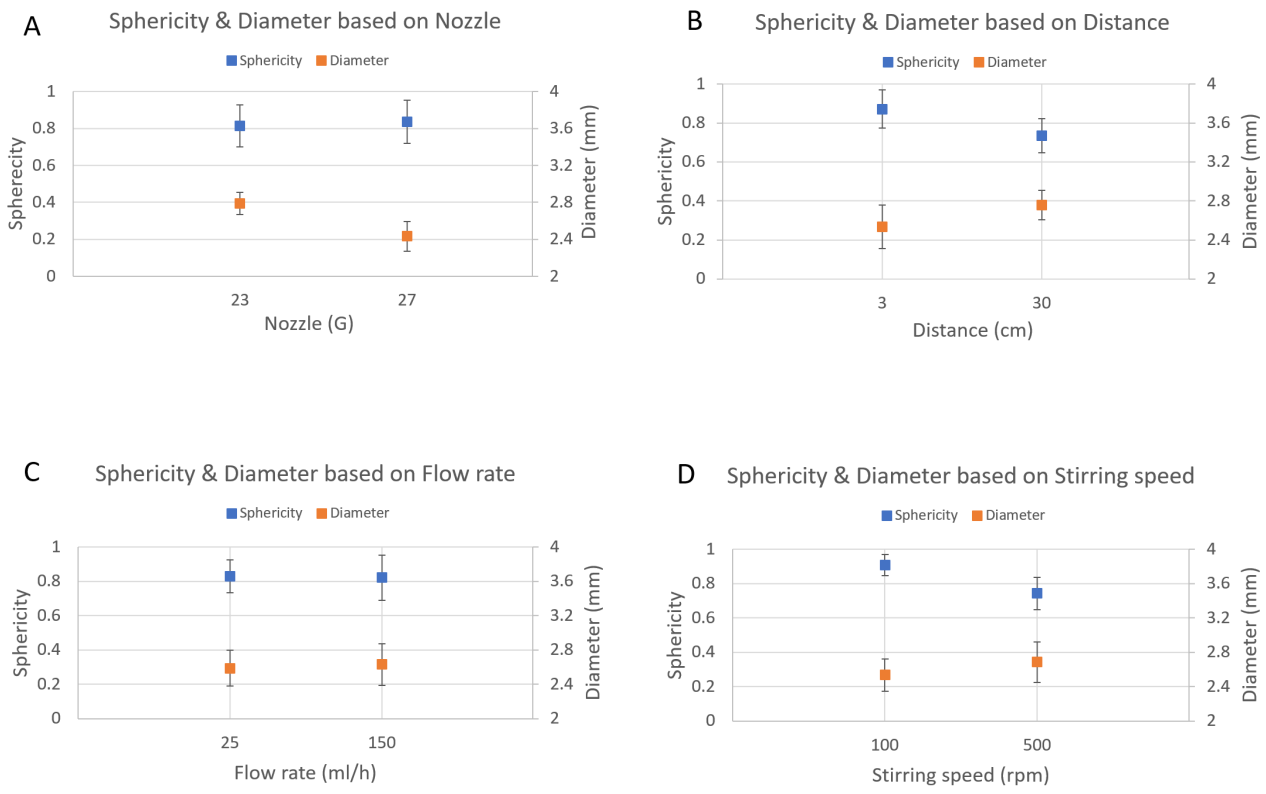

Figure 3.1: Sphericity and diameter of Alginate beads based on nozzle (A), distance (B), flow-rate (C), and stirring speed (D).

Hence, based on these graphs, it can be concluded that the best parameters to obtain the highest sphericity and smallest sizes seem to be 27 G for the nozzle, 3 cm for the distance, and a stirring speed of 100 rpm. The flow rate appears to have minimal impact. This observation corresponds with table 3.1, where the best conditions obtained are from the same parameters and both flow rates. Also, it is

easier to notice that even the lower flow rate shows slightly better outcomes, the standard deviation is also slightly higher.

Figure 3.2 serves as a visual representation for a clearer comparison of size and shape based on nozzle and flow rate. When comparing the nozzle, the difference in bead size is 0.33 mm for both flow rates. On the other hand, comparing flow rates alone results in a variation of just 0.04 mm, with the smallest nozzle and the lowest flow rate showing the most effective reduction in bead size. Focusing now on the sphericity, it is slightly better for the smallest nozzle and the highest flow rate, but no significant variations are observed.

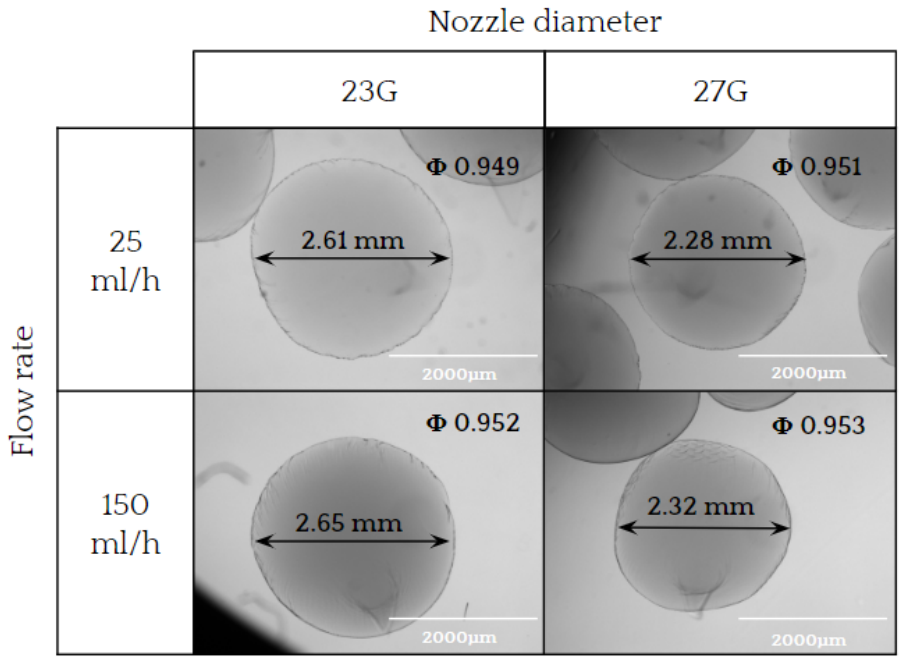

Figure 3.2: Alginate beads produced using a 23G and 27G nozzle, flow rates of 25 mL/h and 150 mL/h, a distance of 3 cm, and a stirring speed of 100 rpm.

Additionally, to study whether there is a correlation between these parameters and the outcome, a statistical test was performed, from which the p-values can be obtained as shown in table 3.2 (See Appendix A for SPSS outcomes).

p-values	**Diameter**	**Sphericity**
Flow rate	0.858	0.128
Nozzle	< 0.001	0.486
Distance	0.002	0.003
Stirring speed	0.013	< 0.001

Table 3.2: Parameter p-values for dependent variables diameter and sphericity obtained through ANOVA in SPSS.

Knowing that when $p < 0.05$ there is a correlation between variables, it is clearly seen that the distance

and stirring speed affect both the diameter and sphericity. And that is why the best conditions have the same distance and stirring speed. Also, the nozzle is related to the diameter, so when the inner diameter is reduced, the diameter of the bead also decreases. Regarding the flow rate, there is no statistical evidence of affecting either the diameter or the sphericity.

3.1.2 Size and sphericity of magnetic Alginate beads

After producing magnetic beads under five different conditions, with different concentrations of alginate and iron, their size and sphericity were evaluated. The average size and sphericity are shown in figure 3.3, along with a visual representation in figure 3.4.

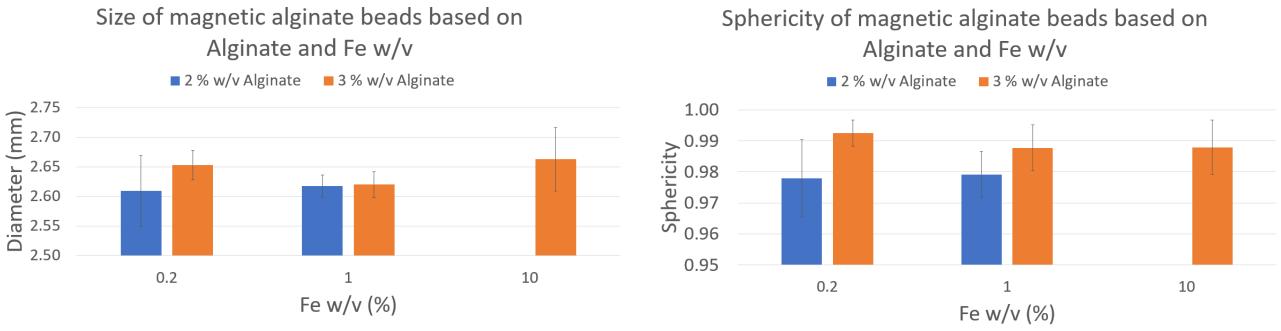

Figure 3.3: Size (left) and sphericity (right) of magnetic alginate beads based on alginate and iron weight fractions.

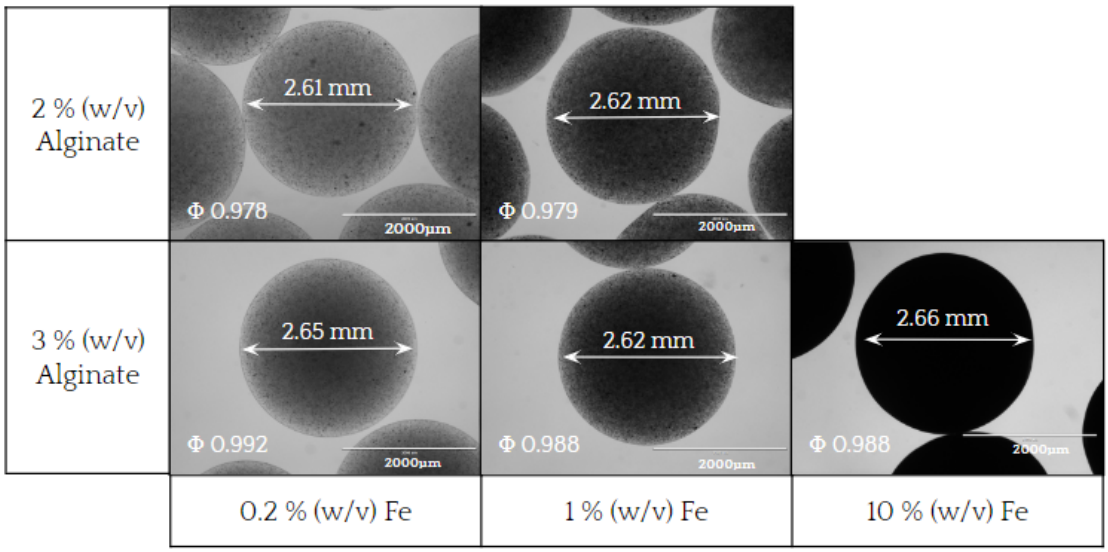

Figure 3.4: Size and sphericity of magnetic alginate beads based on different alginate and iron concentrations.

When comparing the alginate content, there is a small increase in the diameter (0.04 mm) for the 3 % with the lowest iron content. However, this is minimal for the 1 % (w/v) Fe (below 0.01 mm).

For the sphericity, those conditions with higher alginate content obtained a higher rate. If the focus is switched to the Fe content, the size seems to be slightly higher (around 0.04 mm) when increasing the amount of iron considerably (0.2 and 1 % conditions to 10 %), except for the condition with 3% alginate and 0.2 % Fe. While comparing 0.2 with 1 % (w/v) Fe, this observation does not apply as these percentages are closer together. There is no significant remark regarding the sphericity.

Overall, the results obtained show little variability for both the diameter and sphericity. The sizes of all the bead conditions studied are around 2.6 mm in diameter, all with spherical shapes. As increasing the viscosity of the solution improves the homogeneity of the Fe distribution, the beads produced with 3% (w/v) of alginate and different iron content were the ones employed to study their magnetic properties.

3.1.3 Oxidation state

Diffraction peaks of the magnetic alginate beads at 44°, 64°, 82° and 98° (figure 3.5) match the peaks of the Pure Iron powder and Alpha Iron reference file. The absence of additional peaks in the magnetic alginate beads indicates that the iron is mainly present in its pure state, there are no iron oxides present inside the beads. The peaks of iron inside alginate beads have lower intensity than the pure iron powder peaks, which can be explained by the low percentage of iron inside the analyzed sample compared to the pure iron one. Therefore, the XRD analysis confirmed that the bead production process did not oxide the iron powder.

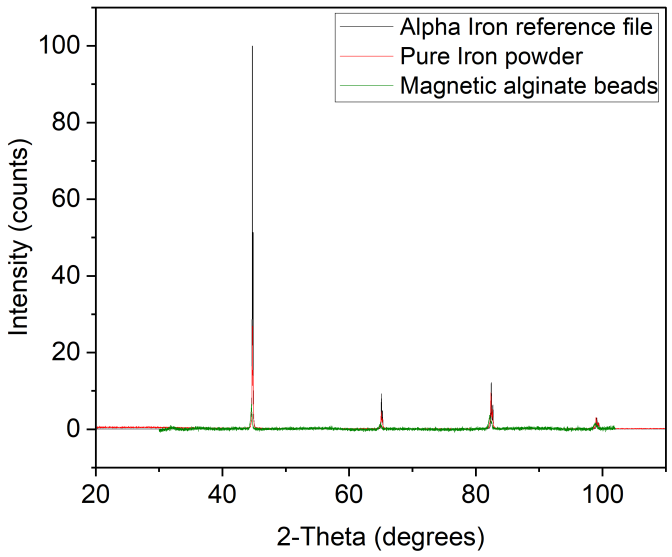

Figure 3.5: XRD diffractogram of magnetic alginate beads compared to Alpha Iron and Pure Iron powder

3.1.4 Magnetic properties

Variations in iron content and solution viscosities were evaluated to gain insights into their influence on the beads' magnetic behavior. Beads with 0.2, 1, and 10 % (w/v) were introduced in solution

viscosities of 1, 10, and 100 cST. Once the beads were magnetically activated, their moving speed was measured. The same beads were used afterward for VSM analysis to measure their actual iron w/v.

3.1.4.1 Moving speed

Moving speeds based on Fe content and solution viscosities are reprsented in the heat map of figure 3.6, along with the graph of figure 3.7 for a different visualization. The speed increases with the Fe content and decreases for higher viscosities, as would be expected.

Apart from this, it was observed that the solution's viscosity has more effect on the bead's moving speed than its Fe w/v. For example, 1% Fe - 1 cST and 10% Fe - 100 cST. Their moving speeds are 35.55 and 25.77 mm/s respectively, being higher when the viscosity is lower and not when the Fe is higher. The viscosity seems to influence the moving speed more than the Fe content. The same trend is evident when the focus is set on values that are relatively close to each other. Conditions 0.2% Fe - 10 cST and 1% Fe - 100 cST have a difference speed of 2.31 mm/s. Similarly happens with conditions 1% Fe - 1 cST and 10% Fe - 10 cST, having a difference of 4.27 mm/s. These little variations suggest that equivalent speeds can be reached with lower Fe - lower viscosities and higher Fe - higher viscosities.

Speed (mm/s)	0.2 % Fe	1 % Fe	10 % Fe
1 cST	17.91	35.55	42.49
10 cST	7.22	20.80	39.82
100 cST	6.01	9.53	25.77

Figure 3.6: Moving speed heatmap of magnetic alginate beads based on different iron content in different solution viscosities.

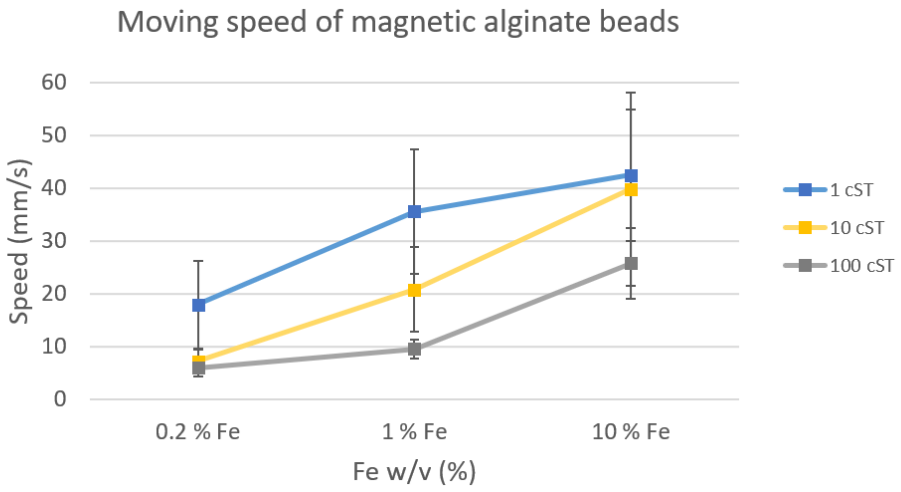

Figure 3.7: Moving speed of magnetic alginate beads based on different iron content in different solution viscosities.

However, the standard deviation of the data (Fig. 3.7) is particularly high. This is due to the inconsistency of the measurements as the magnet was placed manually at different starting distances. Consequently, the movement of the beads measured occurred between 0.1 and 0.6 seconds within the same condition, which influenced the speed variability as the acceleration could not be taken into account. If only the conditions measured at the same time point were considered, the standard deviation

would have been reduced significantly.

In general, the data obtained revealed a clear trend in the relationship between the Fe content and the viscosity, where lower viscosity had a more pronounced effect on increasing speed than higher Fe content. To enhance the reliability of the results and reduce the standard deviation for more accurate data, a consistent method where the magnet could be placed and moved in the same controllable manner for each condition should be designed.

3.1.4.2 VSM analysis

As it is confirmed that the Fe within the beads is not oxidated (iron oxides have different magnetic properties than pure iron), the VSM analysis of pure Fe can be used to determine the actual Fe weight fractions that the beads contain. From the hysteresis curves of pure iron we measured (see Appendix B), the magnetic saturation of 0.022, 0.028, 0.036, and 0.053 g of Fe was obtained. From these data points, a regression model was derived (Figure 3.8). With a coefficient of determination R^2 equal to 0.9995, we can confirm that the magnetic moment saturation is proportional to the iron content in the capsule.

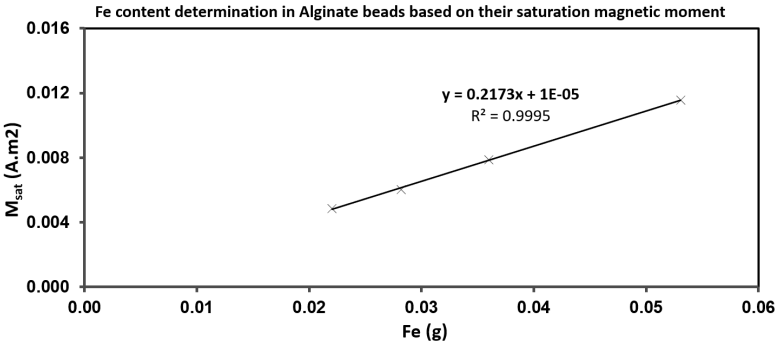

Figure 3.8: Regresion model equation to correlate magnetic saturation with pure Fe content.

From the hysteresis curves of Alginate-Fe beads, where 5 beads were measured for each condition (Figure 3.9), the maximum magnetic moment (magnetic saturation) was measured. Substituting this value into the equation of figure 3.8 and solving for x, the iron content per VSM sample analyzed was determined, making it possible to calculate indirectly the actual Fe weight fractions, as shown in table 3.3.

	0.2 % Fe	1 % Fe	10 % Fe
Fe w/v (%) measured	0.094 ± 0.016	0.744 ± 0.021	9.780 ± 0.182

Table 3.3: Actual iron w/v (%) within magnetic alginate beads (average ± SD) obtained from VSM analysis.

The weight fraction differences reveal a reduction of 53 %, 25.6 %, and 2.2 % for the initial concentrations of 0.2 %, 1 %, and 10 % respectively. The amount of the initially added iron did not integrate completely into the beads during the synthesis process, probably due to the sedimentation of the iron in the syringe. For the lowest weight fraction, this reduction is considerably high, whereas for the highest one, it is negligible. A logarithmic relation may exist between the iron weight fraction and the

reduction percentage. However, further investigation is required to draw stronger conclusions.

These findings suggest that the synthesis process is effective in incorporating iron into the beads, with the iron content reduced compared to the initial concentration. Also, the deviation of the data will be taken into consideration when producing future batches. Consequently, the outcomes obtained in the moving speed are not affected by disproportional Fe content within the beads.

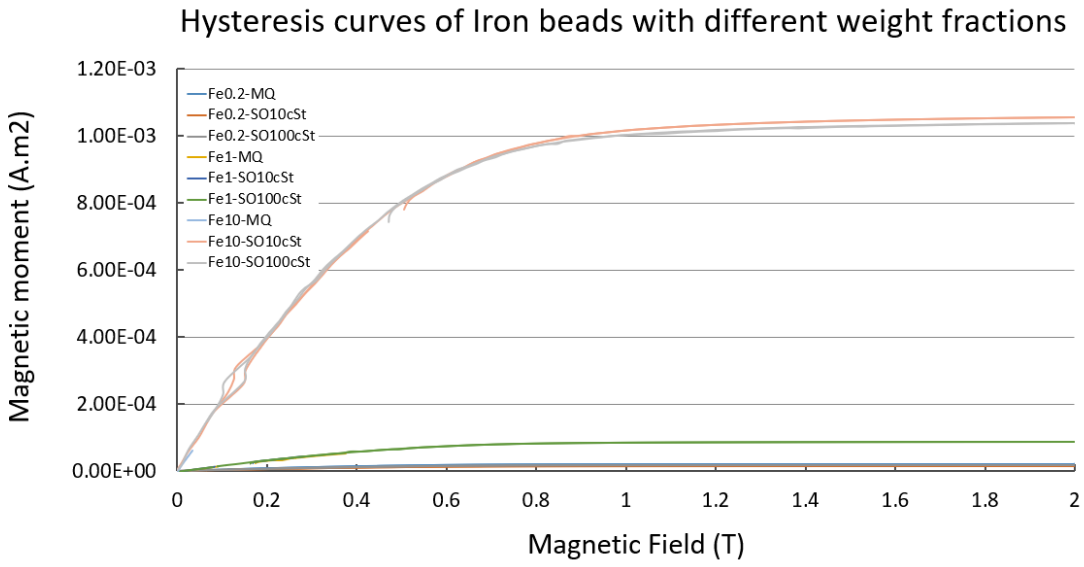

Figure 3.9: Hysteresis curves of Fe beads with different weight fractions analyzed in different solution viscosities

3.2 Biocompatibility of magnetic alginate beads

To assess the biocompatibility of the magnetic alginate beads (1% w/v Fe), C2C12 myoblast cells were cultured in contact with the beads for 1, 3 and 7 days. Also, microcarriers were used to suspend the cells to avoid the cell attachment to the bottom of the well to facilitate mechanical stimulation. Different approaches for the cell attachment to microcarriers were evaluated. Additionally, a live-dead assay was performed to provide a qualitative assessment of cell viability, along with a quantitative analysis to determine the impact of the beads on cells.

3.2.1 Cell attachment to microcarriers

Different approaches were investigated to find the optimal procedure to attach cells to microcarriers. Various combinations of incubation, vortexing, and the use of a roller mixer were tested to assess improvements in cell attachment. Results are depicted in figure 3.10. The different solution conditions analyzed under the microscope contained just a few microcarriers and the difference in cell attachment is difficult to discern. Regardless, each condition appears to be effective for cell attachment as cells exhibited good adherence to the microcarriers, represented as the mosaic patterns that can be visualized. Consequently, as there are no significant differences observed, the procedure for the cell attachment established was the incubation for 2 hours, chosen for its reduced workload.

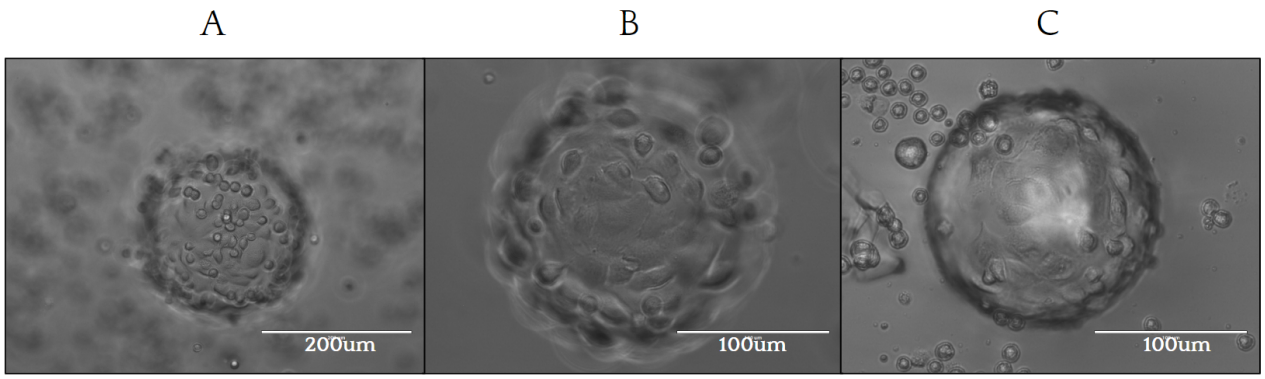

Figure 3.10: Cell attachment to microcarriers: A) Incubation for 2h; B)Incubation for 2h vortexing every 30 minutes for 10 seconds; C)Incubation for 2h and roller mixing every 30 minutes for 2 minutes.

3.2.2 Live Dead Assay and Cell viability

Before performing the live-dead staining, each condition was examined under the microscope, revealing the presence of bead fragments outside the bead (Fig. 3.11 - Before). Despite this, the iron particles remained entrapped within the alginate structure. Also, for the time point day 1, conditions were washed with PBS before the staining, which caused the decrosslinking of the alginate beads (Fig. 3.11 - After). For the rest of the time points, rinsing with PBS was avoided to prevent bead dissolution, as it was found in the literature that PBS causes the decrosslinking of the alginate by sodium ions replacing the calcium ones [49].

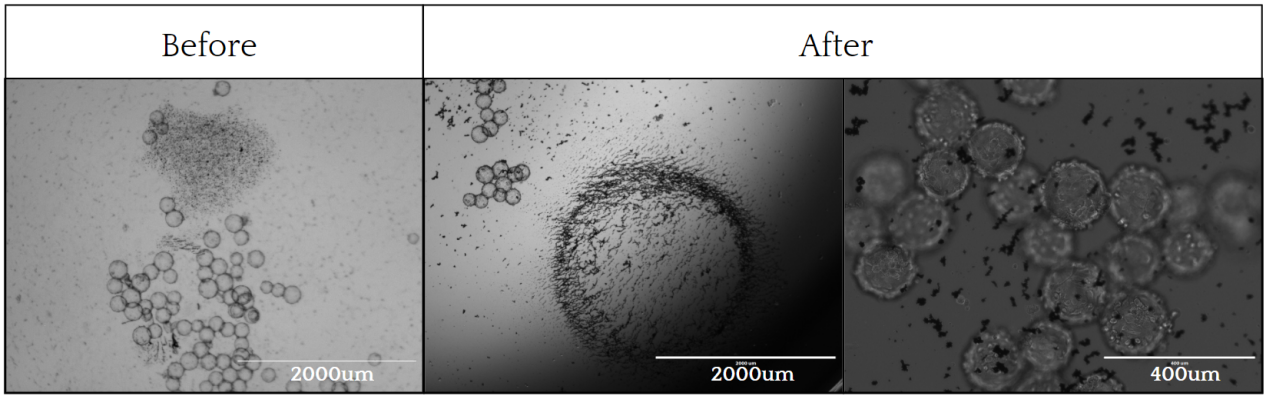

Figure 3.11: Bead condition before (no PBS) and after (rinsed with PBS) the live-dead staining on day 1.

Live-dead assay performed after 1, 3 and 7 days (Fig. 3.12) reported the presence of live cells, indicating that the broken bead did not compromise the viability of the cells. This suggests the resilience of the cells upon the iron leakage. However, on days 3 and 7, PBS was avoided and the iron seemed to be trapped inside the alginate despite the bead being broken down. Cells likely did not come into direct contact with the iron, which would explain their viability.

Aside from this, the fluorescence signal is partially overlapped, which means that the live-dead assay may not provide an accurate contrast between live and dead cells. This overlapped signal can be

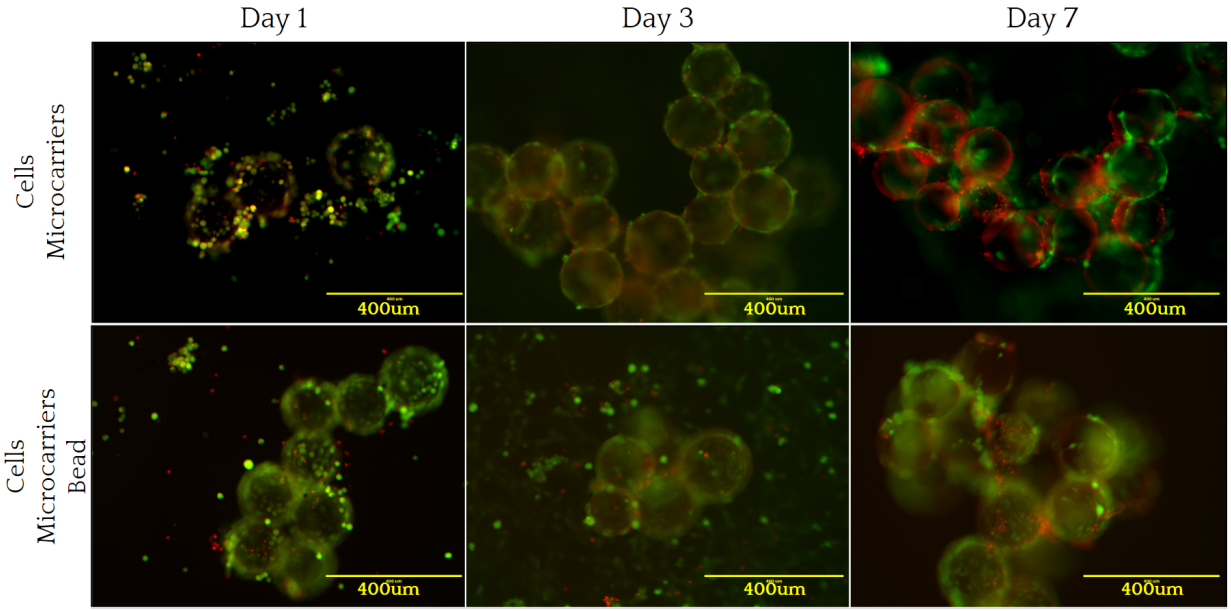

Figure 3.12: Fluorescence microscopy images of Live/Dead assay. Cells attached to microcarriers with and without the bead after 1, 3 and 7 days.

atributed to the similar wavelengths of the fluorophores, detecting both live and dead fluorescence signals simultaneously. This is translated into a yellow fluorescence when the images are merged.

When multiple beads were in combiation with cells (Fig. 3.13), regardless of whether in contact with PBS (day 1) or not (day 3), cells remained alive. Remarkably, cells not only surrounded the beads, but also attached to the Fe-alginate fragments of the broken beads. This observation also supports the high cell viability observed despite the breakage of the beads. The limited fluorescence signals (some cells do not seem to emit fluorescence) might be due to the image processing. Combining the images with a grey background affected the visibility of the signals, reducing the contrast. It is also possible that the staining may not be efficient, leading to variations in signal intensity, or the outcome may have been influenced by human or technical error.

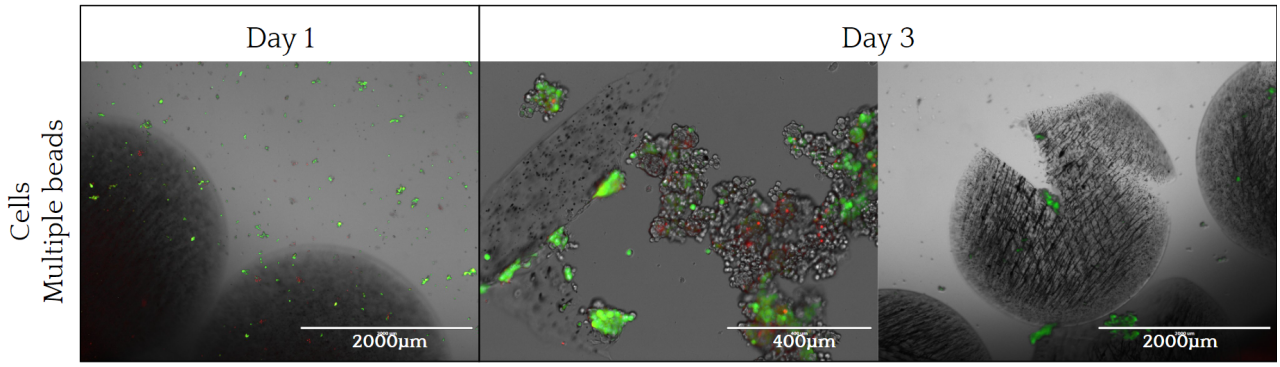

Figure 3.13: Fluorescence microscopy images of Live/Dead assay. Cells with multiple beads after 1 and 3 days.

Finally, cells were manually counted after being cultured for 1, 3 and 7 days to provide a quantitative measurement (see Fig. 3.14. The extremely high outcome for the condition 'cells - day 1' probably involves a human error in cell counting, as cells typically do not grow more than twice their initial density. The condition 'cells + bead' shows an ascendent trendline maintained underneath the control, meaning that the cell viability is slightly reduced when the magnetic bead is present.

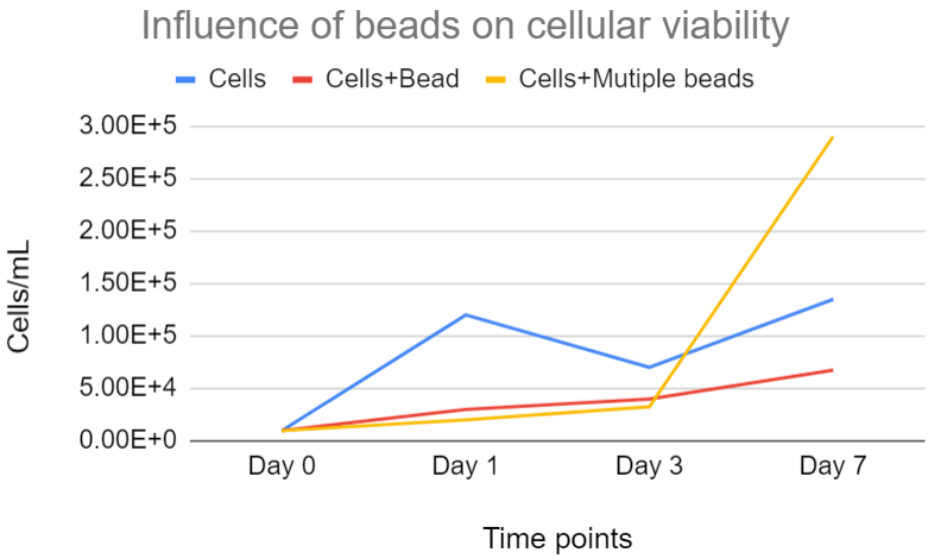

Figure 3.14: Cellular viability based on beads presence.

Moreover, from day 0 until day 3, the same happens for 'cells + multiple beads'. This correlation indicates that the cell viability decreases with an increasing number of magnetic beads. On day 7, however, the amount of cells grows drastically, rising above the rest of the conditions. This unpredicted outcome could be because of the same reason as the other unexpected value, a technical or human interference. The cell viability on day 7 could be calculated as dead cells were also counted, obtaining 61, 60 and 75 % for 'cells', 'cells + bead' and 'cells + multiple beads' respectively.

Although the cell viability is reduced under the presence of magnetic beads, the live-dead assay proved a robust cell survival even with the decrosslinking and breakage of the beads. However, further optimization for both qualitative and quantitative processes should be addressed to improve the accuracy of the assay and cell viability.

4

Conclusions

Considering the challenges in tissue engineering, magnetic alginate beads might be used to stimulate cells mechanically to influence cell fate and differentiation for regenerative medicine. These beads can be successfully synthesized through extrusion dripping, although the method could be improved to obtain more homogenous Fe-alginate beads.

Their size and sphericity can be controlled through the syringe pump setup parameters. The nozzle's inner diameter has a direct impact on the bead size. Also, the distance between the nozzle and the surface of the crosslinking bath influences both outcomes, improving the results when this distance is closer to the minimum value possible. The iron content did not provide clear evidence of influencing the size or shape of the beads. When varying iron content in future studies, its impact on bead characteristics should be assessed.

Exploring the beads' magnetic properties, we find that the encapsulated iron does not oxide during the synthesis process. Furthermore, the solution viscosity in which the beads were evaluated is a more influential factor than the Fe content concerning moving speeds. However, it was also discovered that the actual weight fraction of Fe present in the beads is lower than the initial one due to iron sedimentation. This factor needs to be considered and prevented as much as possible to enhance the homogeneity.

As for their biocompatibility, an appropriate cell viability was observed, taking into account the bead's degradability. Despite the Fe being trapped inside alginate fragments, the bead's breakage decreases the cell viability. However, for more accurate results, especially in moving speeds and cell viability, it is advisable to repeat experiments under more controllable conditions.

In the end, the applicability of magnetic alginate beads remains uncertain since the evaluation of the impact of magnetic stimulation on cell behavior was not accomplished, unfortunately, due to limitations in time. Future investigations are needed to assess their potential application in tissue engineering.

5

Future perspectives

To improve the observed results, we suggest first further optimization of the magnetic alginate beads production, aiming to reduce their size if necessary and enhance iron distribution. One strategy could be to apply an external force to break them before extrusion from the syringe pump. Also, exploring other production methods, such as microfluidic devices, could be beneficial for applications demanding smaller bead sizes, such as cell encapsulation or drug delivery.

Better controlled experimental conditions are required. Repeating experiments under more controlled conditions would contribute to the accuracy and reliability of the results, particularly for measuring the bead's magnetic responsiveness. To accurately compare their magnetic responses in different solution viscosities, a controlled setup ensuring the same uniform conditions is necessary.

Further research regarding biocompatibility needs to be done to prevent the bead's degradability while in contact with the culture medium. It is crucial to note that the medium should be free of cations, as they contribute to the decrosslinking of alginate. Once the integrity of the beads is not affected, their biocompatibility should be assessed again.

Finally, the impact of magnetic stimulation on cell behavior should be investigated. Designing a strategy that allows controlled stimulation of the magnetic beads would provide insights into the mechanical stimulation of cells. Contributing to the understanding of cellular responses to external stimuli could help to the improvement of the current state of tissue engineering.

References

[1] A. J. Salgado, J. M. Oliveira, A. Martins, F. G. Teixeira, N. A. Silva, N. M. Neves, N. Sousa, and R. L. Reis, "Tissue engineering and regenerative medicine: past, present, and future," *International review of neurobiology*, vol. 108, pp. 1–33, 2013.

[2] F. P. Luyten and J. Vanlauwe, "Tissue engineering approaches for osteoarthritis," *Bone*, vol. 51, no. 2, pp. 289–296, 2012.

[3] T. Ghassemi, A. Shahroodi, M. H. Ebrahimzadeh, A. Mousavian, J. Movaffagh, and A. Moradi, "Current concepts in scaffolding for bone tissue engineering," *Archives of bone and joint surgery*, vol. 6, no. 2, p. 90, 2018.

[4] A. W. C. Chua, Y. C. Khoo, B. K. Tan, K. C. Tan, C. L. Foo, and S. J. Chong, "Skin tissue engineering advances in severe burns: review and therapeutic applications," *Burns & trauma*, vol. 4, pp. s41038–016, 2016.

[5] A. Hollander, P. Macchiarini, B. Gordijn, and M. Birchall, "The first stem cell-based tissue-engineered organ replacement: implications for regenerative medicine and society," 2009.

[6] A. Eder, I. Vollert, A. Hansen, and T. Eschenhagen, "Human engineered heart tissue as a model system for drug testing," *Advanced drug delivery reviews*, vol. 96, pp. 214–224, 2016.

[7] M. He and A. Callanan, "Comparison of methods for whole-organ decellularization in tissue engineering of bioartificial organs," *Tissue Engineering Part B: Reviews*, vol. 19, no. 3, pp. 194–208, 2013.

[8] J. M. Fishman, M. Lowdell, and M. A. Birchall, "Stem cell-based organ replacements—airway and lung tissue engineering," in *Seminars in Pediatric Surgery*, vol. 23, pp. 119–126, Elsevier, 2014.

[9] G. Orlando, P. Baptista, M. Birchall, P. De Coppi, A. Farney, N. K. Guimaraes-Souza, E. Opara, J. Rogers, D. Seliktar, K. Shapira-Schweitzer, *et al.*, "Regenerative medicine as applied to solid organ transplantation: current status and future challenges," *Transplant International*, vol. 24, no. 3, pp. 223–232, 2011.

[10] C. Alberti, "Tissue engineering as innovative chance for organ replacement in radical tumor surgery.," *European Review for Medical & Pharmacological Sciences*, vol. 17, no. 5, 2013.

[11] E. S. Place, J. H. George, C. K. Williams, and M. M. Stevens, "Synthetic polymer scaffolds for tissue engineering," *Chemical society reviews*, vol. 38, no. 4, pp. 1139–1151, 2009.

[12] E. C. Novosel, C. Kleinhans, and P. J. Kluger, "Vascularization is the key challenge in tissue engineering," *Advanced drug delivery reviews*, vol. 63, no. 4-5, pp. 300–311, 2011.

[13] J. Rouwkema, B. F. Koopman, C. A. V. Blitterswijk, W. J. Dhert, and J. Malda, "Supply of nutrients to cells in engineered tissues," *Biotechnology and Genetic Engineering Reviews*, vol. 26, no. 1, pp. 163–178, 2009.

[14] J. Barthes, H. Özçelik, M. Hindié, A. Ndreu-Halili, A. Hasan, and N. E. Vrana, "Cell microenvironment engineering and monitoring for tissue engineering and regenerative medicine: The recent advances," *BioMed Research International*, vol. 2014, p. 921905, 2014.

[15] M. Ermis, E. Antmen, and V. Hasirci, "Micro and nanofabrication methods to control cell-substrate interactions and cell behavior: A review from the tissue engineering perspective," *Bioactive materials*, vol. 3, no. 3, pp. 355–369, 2018.

[16] Y. Ikada, "Challenges in tissue engineering," *Journal of the Royal Society Interface*, vol. 3, no. 10, pp. 589–601, 2006.

[17] Novus biologicals website. Available at `https://www.novusbio.com/research-areas/stem-cells`.

[18] H. D. Zomer, A. S. Vidane, N. N. Goncalves, and C. E. Ambrosio, "Mesenchymal and induced pluripotent stem cells: general insights and clinical perspectives," *Stem cells and cloning: advances and applications*, pp. 125–134, 2015.

[19] B. Bhaskar, N. K. Mekala, R. R. Baadhe, and P. S. Rao, "Role of signaling pathways in mesenchymal stem cell differentiation," *Curr Stem Cell Res Ther*, vol. 9, no. 6, pp. 508–512, 2014.

[20] R. S. Knecht, C. H. Bucher, S. Van Linthout, C. Tschöpe, K. Schmidt-Bleek, and G. N. Duda, "Mechanobiological principles influence the immune response in regeneration: implications for bone healing," *Frontiers in Bioengineering and Biotechnology*, vol. 9, p. 81, 2021.

[21] J.-H. Park, T. Ushida, and T. Akimoto, "Control of cell differentiation by mechanical stress," *The journal of physical fitness and sports medicine*, vol. 2, no. 1, pp. 49–62, 2013.

[22] M. d'Angelo, E. Benedetti, M. G. Tupone, M. Catanesi, V. Castelli, A. Antonosante, and A. Cimini, "The role of stiffness in cell reprogramming: a potential role for biomaterials in inducing tissue regeneration," *Cells*, vol. 8, no. 9, p. 1036, 2019.

[23] J. Spangenberg, D. Kilian, C. Czichy, T. Ahlfeld, A. Lode, S. Gunther, S. Odenbach, and M. Gelinsky, "Bioprinting of magnetically deformable scaffolds," *ACS Biomaterials Science & Engineering*, vol. 7, no. 2, pp. 648–662, 2021.

[24] M. Chighizola, T. Dini, C. Lenardi, P. Milani, A. Podestà, and C. Schulte, "Mechanotransduction in neuronal cell development and functioning," *Biophysical Reviews*, vol. 11, pp. 701–720, 2019.

[25] B. D. Matthews, D. R. Overby, R. Mannix, and D. E. Ingber, "Cellular adaptation to mechanical stress: role of integrins, rho, cytoskeletal tension and mechanosensitive ion channels," *Journal of cell science*, vol. 119, no. 3, pp. 508–518, 2006.

[26] H.-C. Chen and Y.-C. Hu, "Bioreactors for tissue engineering," *Biotechnology letters*, vol. 28, pp. 1415–1423, 2006.

[27] C. Czichy and S. Odenbach, "Modelling of the deformation behaviour of a magnetic hydrogel in a magnetic field gradient," *Smart Materials and Structures*, vol. 32, no. 11, p. 115008, 2023.

[28] S. Kondaveeti, A. T. S. Semeano, D. R. Cornejo, H. Ulrich, and D. F. S. Petri, "Magnetic hydrogels for levodopa release and cell stimulation triggered by external magnetic field," *Colloids and Surfaces B: Biointerfaces*, vol. 167, pp. 415–424, 2018.

[29] C. S. d. Lima, T. S. Balogh, J. P. Varca, G. H. Varca, A. B. Lugão, L. A. Camacho-Cruz, E. Bucio, and S. S. Kadlubowski, "An updated review of macro, micro, and nanostructured hydrogels for biomedical and pharmaceutical applications," *Pharmaceutics*, vol. 12, no. 10, p. 970, 2020.

[30] N. Farshidfar, S. Iravani, and R. S. Varma, "Alginate-based biomaterials in tissue engineering and regenerative medicine," *Marine Drugs*, vol. 21, no. 3, p. 189, 2023.

[31] G. Liling, Z. Di, X. Jiachao, G. Xin, F. Xiaoting, and Z. Qing, "Effects of ionic crosslinking on physical and mechanical properties of alginate mulching films," *Carbohydrate polymers*, vol. 136, pp. 259–265, 2016.

[32] J. Li, J. He, Y. Huang, D. Li, and X. Chen, "Improving surface and mechanical properties of alginate films by using ethanol as a co-solvent during external gelation," *Carbohydrate polymers*, vol. 123, pp. 208–216, 2015.

[33] J. Lima, A. I. Gonçalves, M. T. Rodrigues, R. L. Reis, and M. E. Gomes, "The effect of magnetic stimulation on the osteogenic and chondrogenic differentiation of human stem cells derived from the adipose tissue (hascs)," *Journal of Magnetism and Magnetic Materials*, vol. 393, pp. 526–536, 2015.

[34] C. Xiao, P. Ma, and N. Geng, "Multi-responsive methylcellulose/fe-alginate-g-pva/pva/fe3o4 microgels for immobilizing enzyme," *Polymers for Advanced Technologies*, vol. 22, no. 12, pp. 2649–2652, 2011.

[35] A. M. Alshehri, O. C. Wilson Jr, B. Dahal, J. Philip, X. Luo, and C. B. Raub, "Magnetic nanoparticle-loaded alginate beads for local micro-actuation of in vitro tissue constructs," *Colloids and Surfaces B: Biointerfaces*, vol. 159, pp. 945–955, 2017.

[36] B.-B. Lee, P. Ravindra, and E.-S. Chan, "Size and shape of calcium alginate beads produced by extrusion dripping," *Chemical Engineering & Technology*, vol. 36, no. 10, pp. 1627–1642, 2013.

[37] F. Davarcı, D. Turan, B. Ozcelik, and D. Poncelet, "The influence of solution viscosities and surface tension on calcium-alginate microbead formation using dripping technique," *Food Hydrocolloids*, vol. 62, pp. 119–127, 2017.

[38] Handymath website for concentration calculations. Available at `https://tinyurl.com/Handymath`.

[39] H. Khan, A. S. Yerramilli, A. D'Oliveira, T. L. Alford, D. C. Boffito, and G. S. Patience, "Experimental methods in chemical engineering: X-ray diffraction spectroscopy—xrd," *The Canadian journal of chemical engineering*, vol. 98, no. 6, pp. 1255–1266, 2020.

[40] Y. Krisnandi, F. Yanti, and S. Murti, "Synthesis of zsm-5 zeolite from coal fly ash and rice husk: characterization and application for partial oxidation of methane to methanol," in *IOP Conference Series: Materials Science and Engineering*, vol. 188, p. 012031, IOP Publishing, 2017.

[41] B. Gurzęda, P. Florczak, M. Kempiński, B. Peplińska, P. Krawczyk, and S. Jurga, "Synthesis of graphite oxide by electrochemical oxidation in aqueous perchloric acid," *Carbon*, vol. 100, pp. 540–545, 2016.

[42] Bruker X-ray Diffractometers website. Available at `https://www.bruker.com/en/products-and-solutions/diffractometers-and-x-ray-microscopes/x-ray-diffractometers/d8-discover-family.html`.

[43] P. A. Janmey, D. A. Fletcher, and C. A. Reinhart-King, "Stiffness sensing by cells," *Physiological reviews*, vol. 100, no. 2, pp. 695–724, 2020.

[44] B. Kirupakar, B. Vishwanath, M. P. Sree, and D. Deenadayalan, "Vibrating sample magnetometer and its application in characterisation of magnetic property of the anti cancer drug magnetic microspheres," *International Journal of Pharmaceutics and Drug Analysis*, vol. 4, no. 5, pp. 227–233, 2016.

[45] P. H. Jakob, J. Kehrer, P. Flood, C. Wiegel, U. Haselmann, M. Meissner, E. H. Stelzer, and E. G. Reynaud, "A 3-d cell culture system to study epithelia functions using microcarriers," *Cytotechnology*, vol. 68, pp. 1813–1825, 2016.

[46] P. Treenate and P. Monvisade, "Crosslinker effects on properties of hydroxyethylacryl chitosan/sodium alginate hydrogel films," in *Macromolecular Symposia*, vol. 372, pp. 147–153, Wiley Online Library, 2017.

[47] D. Bratosin, L. Mitrofan, C. Palii, J. Estaquier, and J. Montreuil, "Novel fluorescence assay using calcein-am for the determination of human erythrocyte viability and aging," *Cytometry Part A: the journal of the International Society for Analytical Cytology*, vol. 66, no. 1, pp. 78–84, 2005.

[48] S. Zhou, Z. Cui, and J. Urban, "Dead cell counts during serum cultivation are underestimated by the fluorescent live/dead assay," tech. rep., Wiley Online Library, 2011.

[49] E. Baldwin, K. Russell, L. A. Wells, *et al.*, "Dna-crosslinked alginate and layered microspheres to modulate the release of encapsulated fitc-dextran," *European Journal of Pharmaceutics and Biopharmaceutics*, vol. 158, pp. 313–322, 2021.

Appendix

A SPSS analysis procedure and outcome

The process followed in SPSS for the statistical analysis is as follows:

1. Open SPSS software.
2. Insert the data from Table 3.1.
3. Go to **Analyze** → **General Linear Model** → **Univariate**.
4. Select 'Diameter' as the dependent variable and 'Nozzle', 'Distance', 'Flow rate' and 'Stirring speed' as Fixed Factors.
5. Click on **Model** → **Build terms**
6. Change 'Type': from 'Interaction' to 'Main effects' to avoid the interaction between independent variables.
7. Select 'Nozzle', 'Distance', 'Flow rate' and 'Stirring speed' from Factors & Covariates and click on the right blue arrow to move them to the model.
8. Click on **Continue** → **OK**.
9. The table 'Test of Between-Subjects Effects' will be shown.
10. Repeat the process from step 4 now for the 'Sphericity' as the dependent variable.

The tables 'Test of Between-Subjects Effects' for both 'Diameter' and 'Sphericity' dependent variables, from which p-values were obtained, are shown below:

Tests of Between-Subjects Effects

Dependent Variable: Diameter

Source	Type III Sum of Squares	df	Mean Square	F	Sig.
Corrected Model	,579[a]	4	,145	25,033	<,001
Intercept	74,741	1	74,741	12922,419	<,001
Nozzle	,381	1	,381	65,891	<,001
Distance	,129	1	,129	22,341	,002
Flow_rate	,000	1	,000	,034	,858
Stirring_speed	,063	1	,063	10,952	,013
Error	,040	7	,006		
Total	82,388	12			
Corrected Total	,620	11			

a. R Squared = ,935 (Adjusted R Squared = ,897)

Tests of Between-Subjects Effects

Dependent Variable: Sphericity

Source	Type III Sum of Squares	df	Mean Square	F	Sig.
Corrected Model	,142[a]	4	,035	13,819	,002
Intercept	6,865	1	6,865	2681,681	<,001
Nozzle	,001	1	,001	,540	,486
Distance	,051	1	,051	19,729	,003
Flow_rate	,008	1	,008	2,987	,128
Stirring_speed	,089	1	,089	34,940	<,001
Error	,018	7	,003		
Total	8,331	12			
Corrected Total	,159	11			

a. R Squared = ,888 (Adjusted R Squared = ,823)

B Hysteresis curves of pure Fe obtained from VSM analysis